Chemical Physics 398 (2012) 221–227

Contents lists available at ScienceDirect

Chemical Physics

journal homepage: www.elsevier.com/locate/chemphys

Temporal behavior of line-to-continuum ratios and ion fractions as a means of assessing thermodynamic equilibrium in laser-induced breakdown spectroscopy

Heh-Young Moon [1], Benjamin W. Smith, Nicoló Omenetto *

Department of Chemistry, University of Florida, Gainesville, FL 32611, United States

ARTICLE INFO

Article history:
Available online 23 July 2011

Keywords:
Laser-induced plasma
Local thermodynamic equilibrium
Diagnostic methods
Self-absorption
Ion fraction

ABSTRACT

Two diagnostic approaches, aimed at evaluating the departure from local thermodynamic equilibrium (LTE) in laser-induced plasmas, are discussed in this paper. The first approach is based upon the observed temporal behavior of the ratio between selected atomic transitions and the nearby spectral continuum, while the second approach makes use of the plot of the ion fraction of different elements as a function of their respective ionization potentials. Both approaches are known in atomic emission spectroscopy: the former has been described and used in the case of a high pressure surfatron argon plasma, and the latter follows directly from the classic work dealing with d.c. arc emission in general, and a d.c. copper arc in particular. Such approaches, however, have not yet been applied to laser-induced plasmas. It is shown that the experimental results obtained with both methods agree with those reported in the literature using more conventional approaches. For example, in this work, the well-known outcome that the excitation temperature and the ion (electron) temperature differ substantially at early delays after the formation of the plasma is clearly supported by the line-to-continuum approach applied to atomic and ionic transitions of Cu and Fe. In addition, the agreement between the experimental and theoretical behavior of the ion fraction versus the ionization potential for the elements Cu, Fe, Ni, Mg and Ti improves as the delay time increases.

1. Introduction

In every kind of plasma, the various theoretical expressions describing the system behavior and the resulting radiation are based upon the existence of LTE. It is therefore understandable that several diagnostic approaches have been described and tested with the aim of justifying the LTE assumption. In a recent paper, Cristoforetti et al. [1] have questioned the *mere* use of the McWhirter criterion [2] for checking the existence of LTE in laser-induced plasmas. This seems especially appropriate at early delays after plasma formation, due to the large gradients in temperature and electron number density [3,4]. As a result, a combination of different diagnostic approaches becomes necessary.

Several of these methods have been discussed in the literature (see, e.g., [5–7]). In their recent review, Hahn and Omenetto [5] have proposed a series of correlated measurements to be performed as an LTE validating procedure. Among the approaches proposed, two involve the measurement of the *line-to-continuum ratio* and of the *ion-to-neutral ratio*. To our knowledge, although both approaches are well known in the plasma spectroscopy literature (see, for example, [8–11] for the line-to-continuum approach and [12–22] for the ion-to-neutral ratio) and have been used in laser induced plasma as diagnostic tools to check the departure from LTE conditions, the *specific approaches* described in this paper have been discussed before in the case of a microwave plasma [9] and a d.c. arc [23], but have never been put to test in laser induced plasmas.

The purpose of this paper is therefore to discuss the application of these two specific approaches to an atmospheric pressure laser-induced plasma induced on solid targets.

2. Basic approaches

2.1. Line-to-continuum ratio

The line-to-continuum ratio is a useful parameter in plasma diagnostics. The working expression used here (see Appendix A, for its derivation) is shown below [8,9]:

$$R_{exp}(\lambda) = 2\cdot 10^{-5}\frac{A_{u\ell}g_u}{Z_i}\left(\frac{\lambda}{\Delta\lambda_{meas}}\right)\frac{1}{T_e} \times \frac{\exp\left(\frac{-E_u}{kT_{exc}}\right)\exp\left(\frac{E_i-\Delta E_i}{kT_e}\right)}{\left[\xi\left(1-\exp\frac{-hc}{\lambda kT_e}\right)+G\exp\left(\frac{-hc}{\lambda kT_e}\right)\right]}. \quad (1)$$

* Corresponding author.
E-mail address: omenetto@chem.ufl.edu (N. Omenetto).
[1] Present address: Korea Research Institute of Standards and Science, Yuseong-gu, Daejeon 300-814, Republic of Korea.

0301-0104/$ - see front matter © 2011 Elsevier B.V. All rights reserved.
doi:10.1016/j.chemphys.2011.07.002

In the above expression, $A_{u\ell}$ is the spontaneous transition probability, g_u the statistical weight of the upper level, Z_i the ion partition function, E_u the upper excitation energy of the atomic transition, E_i the ionization potential, ΔE_i the lowering correction term of the ionization potential, λ the wavelength of the atomic transition and of the continuum, $\Delta\lambda_{meas}$ the spectral bandwidth of the monochromator, c the velocity of light and k the Boltzmann constant. All parameters are expressed in SI units. The above relation contains two different temperatures: the excitation temperature (T_{exc}), and the electron temperature (T_e). Following Sola et al. [9], it is assumed here that the ionization temperature (T_i) and the electron temperature (T_e) have rapidly equilibrated (see, e.g., [24]). Moreover, two correction factors, namely the free–free Gaunt factor (G) and the free–bound continuum factor (ξ), are present in the denominator of Eq. (1).

Two considerations are worth noting here: first, the wavelength of the continuum is very close to that of the line, thus eliminating the necessity of calibrating the detection system. Note, however, that this strictly refers only to the line/continuum ratio measurement. In fact, the method uses a value of T_{exc} derived from a Boltzmann plot, which usually requires calibration of the spectral response of the system: as a consequence, the overall approach still requires such calibration. Secondly, in Eq. (1), the line is integrated over the entire emission profile while the continuum spectral radiance is given per unit wavelength [5,8,9]. Since experimentally both line and continuum are spectrally integrated, the spectral bandwidth of the monochromator, $\Delta\lambda_{meas}$ enters the expression of the ratio.

Under the LTE assumption, only one temperature is sufficient and normally used in Eq. (1). Sola et al. [9] were the first to suggest that the two parameters T_e and T_{exc} could be kept different from each other. By measuring T_{exc} independently by the Boltzmann approach, two experimental values are available (T_{exc} and R), which can both be inserted in Eq. (1). T_e can now be calculated and compared with the value of T_{exc} obtained by the Boltzmann plot, using appropriate values of G and ξ. The discrepancy between T_{exc} and T_e can be attributed to a departure from LTE.

This method, in principle, is valid irrespective of the line chosen. In this work, several lines were indeed investigated. We report here the results obtained by using only neutral atomic transitions, since they were found to represent the best compromise in terms of practical delay times used and signal-to-noise ratio obtained.

2.2. Ion-to-neutral ratio

The *ion-to-neutral ratio* approach is derived here from the original work of Corliss in the case of a d.c. copper arc [23]. The formulation of the equation follows that given by Boumans [25] and is reported in Appendix B. The working relation used in this approach is given in Eq. (2) below (cgs units):

$$\log\left[\left(\frac{\alpha_j}{(1-\alpha_j)}\right)\left(\frac{Z_{a,j}}{Z_{i,j}}\right)\right] = \log\frac{S_{n,j}}{n_e} = -\log n_e + \frac{3}{2}\log T - \frac{5040E_{i,j}}{T} + 15.684. \quad (2)$$

In the above equation, reference is made to species j in the plasma. α_j is the degree of ionization, $Z_{a,j}$ and $Z_{i,j}$ are the partition functions of the atom and ions, $S_{n,j}$ is the Saha constant, n_e the electron number density, T the excitation temperature and $E_{i,j}$ the ionization potential. Note that the correction term ΔE_i has been omitted here (see Table 1).

This approach requires the independent measurement of the excitation temperature and electron number density, which can be accomplished using the Saha–Boltzmann method and Stark broadening. From the values of the intensity ratio and the measured Saha–Boltzmann temperature, a graph is constructed by plotting the log of the ion fraction versus the ionization potential of several elements present in the target.

From Eq. (1), one can see that, for a given electron number density (n_e) and corresponding plasma temperature (T), a plot of the ion to neutral ratio (corrected for the partition functions) versus the ionization potential of the atoms should result in a straight line whose slope is determined by T and the intercept is a function of both T and n_e. A family of *theoretical* lines can then be obtained, each valid for one combination of T and n_e, and therefore for *one delay time*. Since this plot is the result of combining expressions valid under equilibrium (Saha and Boltzmann), if such conditions indeed exist, all the elements characterized by different ionization potentials should lie on the theoretical line corresponding to the delay time chosen. Deviation from the line is an indication of the departure from equilibrium conditions.

In analogy with the results of the line-to-continuum ratio approach, one can expect that, also in this case, a better fit would be observed for all elements at longer delays, where equilibrium conditions are more plausible.

3. Experimental

The apparatus used in the present work has been described in detail previously [26]. Briefly, a Nd-YAG laser (Brilliant T27; Quantel USA), 90 mJ/pulse at 1064 nm, 6 ns pulse duration and 1 Hz repetition rate, was focused on the sample surface with a 10 cm focal length quartz lens. All measurements were performed at atmospheric pressure. The overall mechanical adjustments consist in a positioning system, a three-dimensional transition stage for target positioning and a controlled stream of air to carry away the dust plume formed during the interaction.

The plasma emission was focused (at 1:1 magnification) with a 5.0 cm diameter quartz lens, with a focal length of 7.5 cm, onto the entrance slit of an F/6.5 spectrometer (Acton, 0.5 m focal length), equipped with 2400 grooves/mm grating, with a spectral resolution of 0.03–0.05 nm in the spectral range used. A 35 μm slit width was used in all cases. Whenever necessary (for example, for the Cu line at 510.554 nm), cut-off filters were used to eliminate second-order effects. Normally, binning was made over the entire plasma image. The overall detection system was already calibrated for its varying spectral response [26].

The detector is an intensified CCD (ICCD 5764/RB-E, Princeton instruments) with a photosensitive area of 576 × 384 pixels, corresponding to (12.7 × 8.4) mm^2. The spectral coverage by a single pixel varies from 0.016 nm at 282 nm to 0.014 nm at 428 nm. The ICCD is operated by its controller (ST-138, Princeton Instruments) and by a pulse generator (PG-200, Princeton Instruments). The data acquisition was controlled with the Winspec32 software (Version 2.5.18.2, Princeton Instruments). The experimental line profiles were fitted to a Voigt profile: as a general rule, the continuum was evaluated at a distance from the peak assuring that the contribution of the line wings could be safely neglected: in all cases, a minimum distance of approximately five line widths was used.

For the line-to-continuum ratio measurements, a minimum delay time of 50 ns could be used. However, the data obtained at this delay and at delays between 50 and 500 ns were affected by a large uncertainty. The same problem was found at longer delays (3–5 μs), where the continuum intensity could not be measured with an acceptable accuracy. For the ion to neutral ratio, the data obtained at two delays (1 and 5 μs) were compared. All measurements were carried out at atmospheric pressure. The electron number density was calculated from the Stark broadening of the H_α line, using the theoretical expression reported by Hahn and Omenetto in their review [5], while the excitation temperature

Table 1
Spectroscopic parameters of the transitions used for the ion-to-neutral ratio approach.*

Element	λ (nm)	E_ℓ (eV)	E_u (eV)	Z		g_ℓ	g_u	$A_{u\ell}$ (10^{-8}) (Hz)	E_i (eV)	$E_i - \Delta E_i$ (eV)	
				1 μs	5 μs					1 μs	5 μs
Ti(II)	319.087	1.08	4.97	98.4	79.2	6	8	1.3	–	–	–
Ti(I)	319.199	0.02	3.90	147	81.4	7	9	0.85	6.82	6.64	6.68
Ni(II)	230.300	1.16	6.54	26.3	19.4	8	6	2.9	–	–	–
Ni(I)	232.996	0.27	5.59	67.8	43	5	3	5.3	7.63	7.45	7.49
Mg(II)	279.078	4.42	8.86	2.14	2.04	2	4	4.01	–	–	–
Mg(I)	285.213	0	4.35	5.34	1.86	1	3	4.91	7.64	7.46	7.50
Cu(II)	221.811	2.83	8.42	2.75	1.70	5	3	3.41	–	–	–
Cu(I)	282.437	1.39	5.78	7.09	4.21	6	6	0.078	7.72	7.54	7.58
Fe(II)	233.131	0.23	5.55	84.6	67.2	10	8	0.32	–	–	–
Fe(I)	299.951	0.86	4.99	115	62.5	11	11	0.17	7.87	7.69	7.73

* Values were taken from the NIST Atomic Data Base (http://physics.nist.gov, last accessed December 2010), except for the values of Z, which were taken from [33]. The correction term (eV) for the first ionization potential has been calculated from the relation [34]:
$\Delta E_i = 3 \cdot 10^{-8} \left(\frac{n_e}{T}\right)^{1/2}$, where n_e is expressed in cm^{-3} and T in Kelvin. The two Z-values correspond to the two T-values at 1 μs and 5 μs, i.e., 13,671 and 10,031 K, respectively. Similarly, from the measured values of n_e and T at 1 μs and 5 μs delays, the corresponding correction terms were calculated as 0.18 eV and 0.14 eV, respectively.

was calculated from the Saha–Boltzmann approach [5]. Finally, for all the transitions used, self-absorption effects were checked and corrected using the duplicating mirror approach [26].

The targets investigated in this work were a pure copper sample (99.99% Cu) and a standard Al-alloy sample (South African aluminum alloy standards disks, APEX Smelter Co., South Africa) containing 16.05% Cu, 1.27% Mg, 1.09% Fe, 0.53% Ni and 0.17% Ti [26].

4. Results and discussion

4.1. Line to continuum ratio

The electron temperature (T_e) was calculated from the ratio of the wavelength-integrated line intensity to the continuum intensity, taking into account the spectral bandwidth of the monochromator (see Appendix A). As mentioned before, the electron temperature can be calculated by keeping $T_{exc} \neq T_e$ in the theoretical expression given in Eq. (1).

The study was performed on copper with two different samples, i.e., a pure copper metal and an aluminum alloy sample (16.05% Cu). The emission lines selected were free of spectral interference from other lines, while their associated continuum radiation could be measured even at late delay times. Both neutral and ionic lines could be selected. Nevertheless, in the case of ion lines and the copper metal target, two different gate widths and laser energy parameters had to be used in order to prevent saturation of the detector at early delay times. Neutral lines in this case are more useful, being sensitive and observable for a longer period of time. For example, the neutral Cu atomic line at 282.437 nm (in the pure copper metal sample) and 296.112 nm (in the Al-alloy sample) were selected because they produced the highest signal-to-continuum intensity ratio as well as accurately measurable line intensities even at late delay times.

Figs. 1–3 show the temporal behavior of both line and continuum for a large range of delay times (50–1500 ns) and for several copper transitions. A general observation is that, at short delay times (t_d < 300 ns), the excitation temperature cannot be measured accurately because the line emission is embedded in the continuum emission (see, for example, the transition at 465.112 nm in Fig. 3(a)). As a result, it is difficult to discern a clear trend in the temporal behavior of the excitation temperature during this period. When the results of multiple lines are plotted together on the same graph (Fig. 3(b)), the electron temperature exhibits an initial fast decay from about 30,000 K shortly after the plasma formation to about 14,000 K at 5.0 μs. A less pronounced variation is observed from 5.0 to 15 μs, as shown in Fig. 3(b). However, at delays longer than 5.0 μs, the continuum vanishes (see Fig. 3(a)), making the measurement of the line to continuum ratio again inaccurate. Similar trends of plasma temperature were observed in the case of the aluminum alloy sample (Z8). These results illustrate the main drawback of this approach, namely the difficulty of obtaining reliable measurements at delays shorter than 0.5 μs and longer than 5.0 μs.

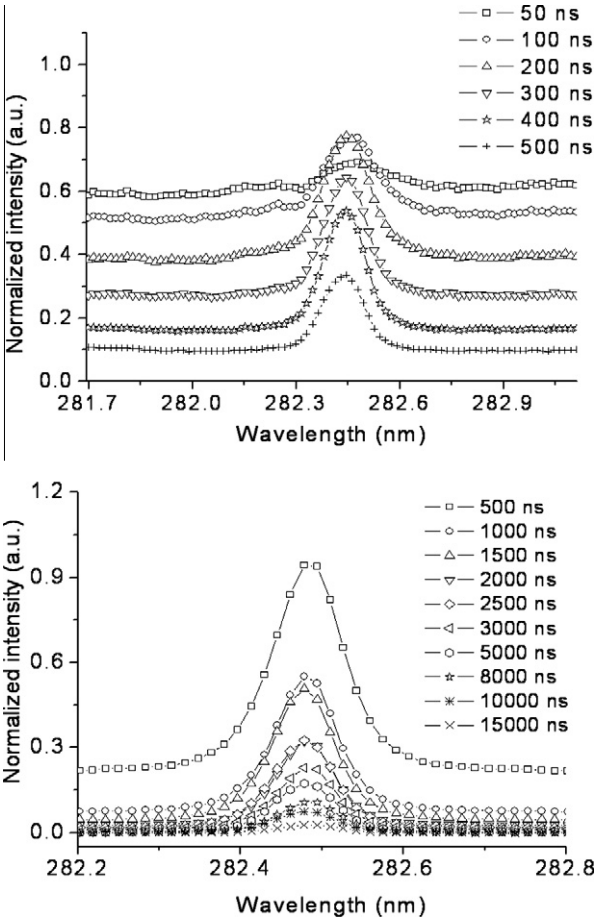

Fig. 1. Spectral behavior in the vicinity of the Cu(I) transition at 282.437 nm at early times (top) and later times (bottom) after plasma formation. A Voigt profile fit is shown in all cases. The drawbacks of the approach are evident here: in the time interval 0–200 ns, the continuum dominates and for time delays longer than 5 μs, the continuum vanishes. Both cases result in very poor signal-to-noise ratios and low accuracy.

From Eq. (1), it can be seen that the Gaunt G (free–free) and Biberman ξ (free–bound) correction factors need to be considered

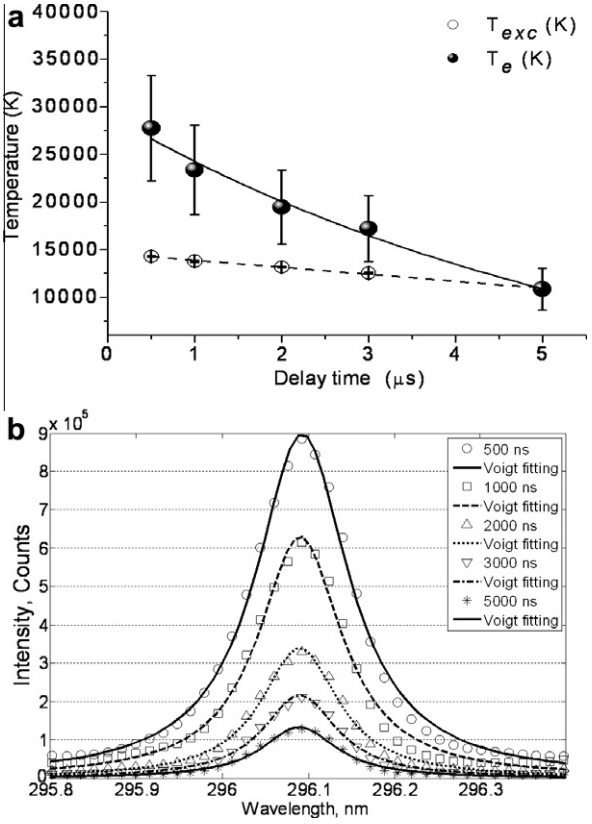

Fig. 2. Experimental behavior of T_e and T_{exc} for a copper atomic transition at 296.12 nm in the time interval 0.5–5 μs. The data shown in (a) confirm the known result that the difference between the excitation and electron temperature decreases with increasing delay times, and that equilibrium conditions are expected at delays around 5 μs and longer. In (b) the line profiles are fitted with a Voigt profile. The denominator of Eq. (1) was neglected here, since both Gaunt and Biberman correction factors were assumed to be unity. *Source:* The top part of this figure was reproduced from Hahn and Omenetto [5], Fig. 7 (with permission from the Society of Applied Spectroscopy).

in the calculations of T_e. If both parameters are equal to 1, the denominator does not play a role since it will be equal to 1. Values of G and ξ are available in the literature and have been measured for different types of plasmas (see, e.g., [8,9,28–32]). In the case of the transitions used in this work (2.4–4.4 eV) and ionization temperatures (considered equal to T_e) of 1–2 eV, the multiplication factor for ξ, i.e., $[1-\exp(-h\nu/kT_e)]$ varies from 0.89 to 0.99. ξ-values very close to unity have been reported for a Kr plasma at $T_e \sim 1$ eV and $n_e \sim 10^{17}$ cm^{-3} [31], while values in the range 0.6–1.6 have been reported for T_e ranging between 1 and 1.3 eV [32]. In our calculation, we have therefore assumed $\xi \sim 1$ and consequently also the first term in the denominator equal to unity. Average G-values in the range 0.04–0.2 have been reported for values of $(h\nu/kT_e)$ ranging between 0.6 and 4 [1,29]. Considering the same range of temperature as above, the multiplication factor for G, i.e., $[\exp(-h\nu/kT_e)]$, will vary in the interval 0.55–0.018. The second term in the denominator of Eq. (1) will then vary from 0.0007 to 0.11. The maximum error expected from assuming the denominator of Eq. (1) being unity is then about 10%.

We have also used here a more pragmatic approach, by calculating the variation of T_e caused by varying G and ξ over a large range (0.01–10), while maintaining the values of T_{exc} and the line-to-continuum ratio fixed. As expected from the above considerations, while the effect of varying G is negligible (except for the 50 ns delay), ξ was found to be causing the largest difference of T_e-values from those calculated for $\xi = 1$. The difference was especially serious (by a factor of ~2) at very early delay times (less than 500 ns) and for high T_e (>40,000 K). However, at delay times greater than 0.5 μs,

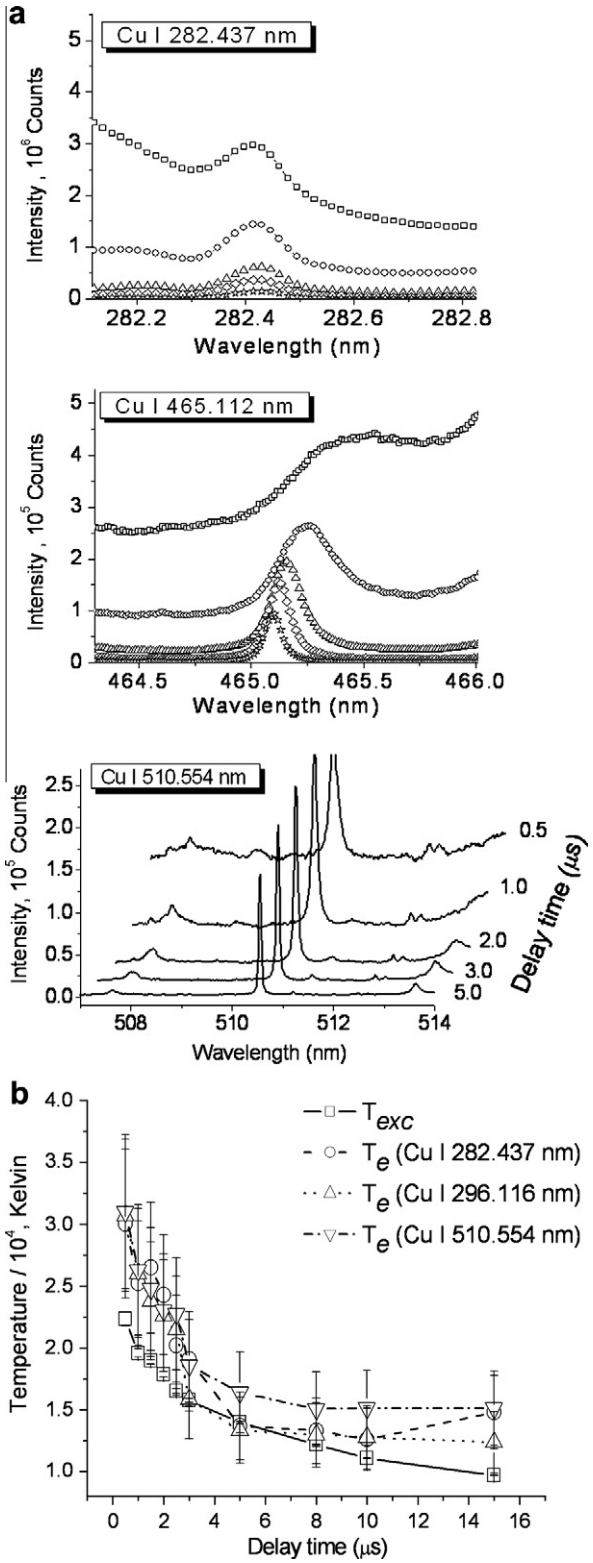

Fig. 3. (a) Spectral line profiles and underlying continuum for three copper transitions chosen for this study in the range of delay times from 0.5 to 5 μs. (b) Experimental behavior of T_{exc} and T_e obtained with an Al alloy target using several neutral copper transitions in the time interval 0.5–5 μs. As explained in the text, and confirmed here, the approach works in principle with any chosen transition. As in the case of Fig. 2, the denominator of Eq. (1) was neglected here, since both Gaunt and Biberman correction factors were assumed to be unity.

and for T_e-values in the range 10,000–25,000 K, the error decreases significantly (to ±10%).

4.2. Ion-neutral ratio

The lines used and the elements investigated with this approach are collected in Table 1. The transition chosen should be free from self-absorption effects: in our case, all the neutral and ionic lines were checked for self-absorption using a duplicating mirror behind the plasma and applying a correction procedure [26,27] (for details, see [26]). The correction factors are collected in Fig. 4(a): their value depends on the concentration of the element in the sample, the transition probability of the line and the energy of the lower level. Moreover, the experimental values of the ion-to-neutral ratios were corrected for the instrumental response of the system [26].

Fig. 4(b) show the experimental results of the application of the Saha–Boltzmann plot at delay times in the range 0.5–5.0 μs. These values, together with the electron number density derived from Stark broadening of the H_α line, have been used to construct the theoretical curves shown in Figs. 5 and 6, with the use of Eq. (2). These figures are the result of measurements carried out at two delay times, i.e., 1.0 and 5.0 μs. The necessity of correcting for self-absorption is evident, in particular in the case of Ti and Mg. As one can see from Fig. 5, showing the data obtained at 1 μs delay, the experimental points lie below the theoretical curve, despite the correction for self-absorption, indicating that the system deviates from LTE. If this is true, and referring also to the results of the line-to-continuum method (see Figs. 2 and 3), a better fit is expected at longer delay times. Fig. 6, which shows the data obtained at 5.0 μs, confirms this expectation, since the data (corrected for self-absorption) are much closer to their predicted theoretical values.

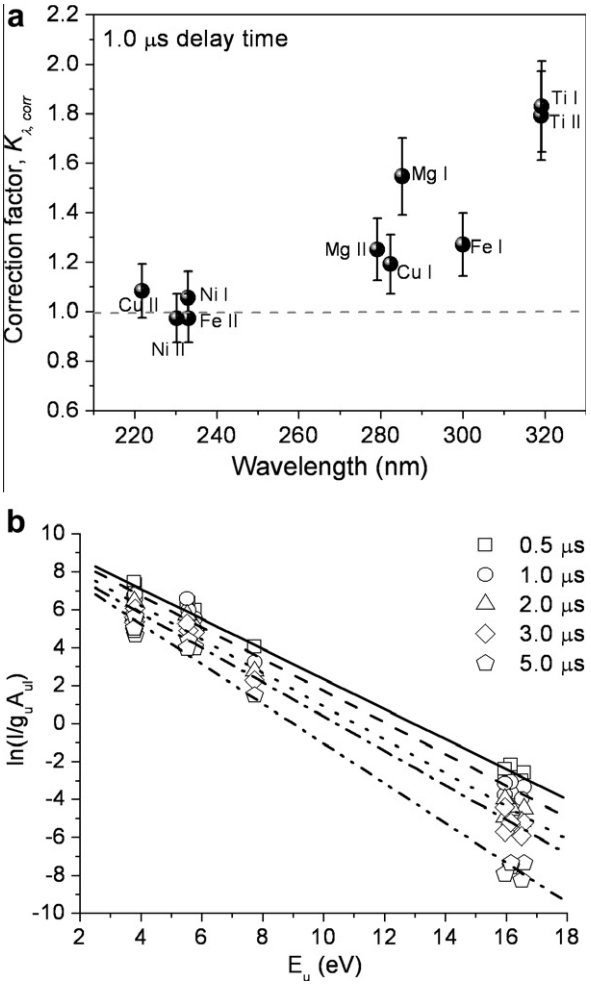

Fig. 4. (a) Experimental values of the self-absorption correction factor for the different elements investigated as determined with the duplicating mirror approach [26]. Both atomic and ionic transitions were used. The data were obtained at 1 μs delay time after plasma formation. (b) Examples of Saha–Boltzmann temperature plots obtained in the time delay range 0.5–5 μs. The corresponding T_{exc} values are: 14,157 K (0.5 μs); 13,671 K (1.0 μs); 12,676 K (2.0 μs); 12,044 K (3.0 μs); 10,031 K (5.0 μs). The standard deviation of the various slopes lies in the range 60–90 K.

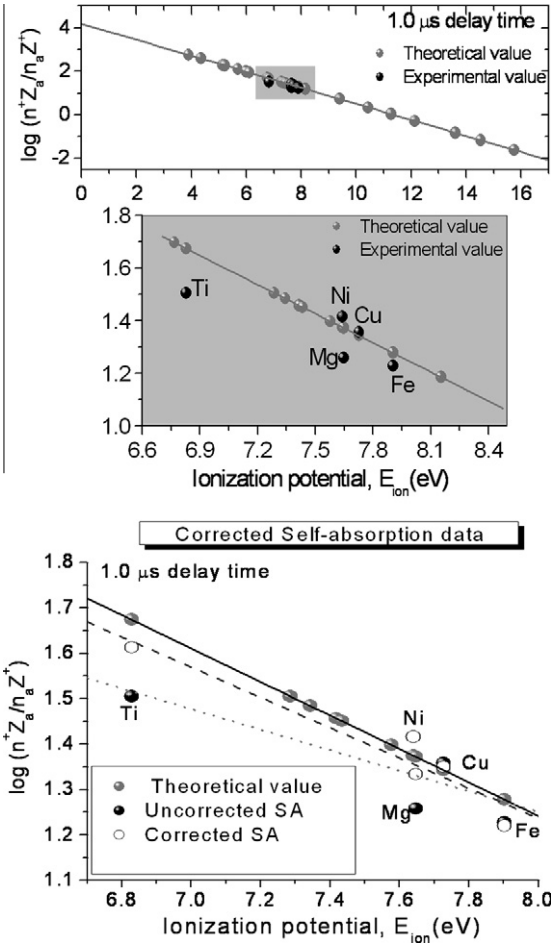

Fig. 5. Comparison between the theoretical and experimental behavior of the ion fraction versus the ionization potential for Ti, Mg, Ni, Cu and Fe. The data refer to a delay time of 1.0 μs. The gray area in the top figure has been expanded in the middle figure to emphasize the difference between theory and experiment. The improvement observed after correcting the data for self-absorption are shown in the bottom graph. The temperature and electron number density for the theoretical curves are 13,671 K and 4.97×10^{17} cm^{-3}. *Source:* The bottom graph of this figure was reproduced from Hahn and Omenetto [5], Fig. 7 (with permission from the Society of Applied Spectroscopy).

A general drawback of the present application of this method is that the range of ionization potentials investigated is rather limited (~1 eV), as indicated by the gray regions of the graphs in both figures. Low E_i-values (e.g., Ba) and high E_i-values (e.g., Zn) should then be added. In the work by Corliss [23], eleven elements were investigated, providing a range of ionization potentials of ~4 eV.

5. Conclusions

This work has demonstrated that the two approaches described can be used to check LTE conditions in laser-induced plasmas. The

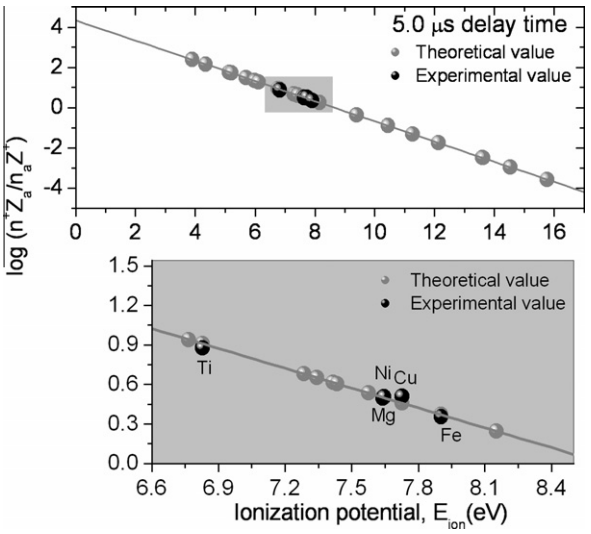

Fig. 6. Comparison between the theoretical and experimental behavior of the ion fraction versus the ionization potential for Ti, Mg, Ni, Cu and Fe. The data refer to a delay time of 5.0 μs. When the graph shown here is compared with that of Fig. 5, obtained at 1 μs delay, the improvement in the agreement between theory and experiment is clearly seen. The experimental data have been corrected for self-absorption. The temperature and electron number density for the theoretical curves are 10,031 K and 2.21×10^{17} cm^{-3}. *Source:* The bottom graph of this figure was reproduced from Hahn and Omenetto [5], Fig. 7 (with permission from the Society of Applied Spectroscopy).

data presented have been obtained on a sufficient number of elements and sufficiently different measurement conditions to warrant justification of this conclusion. On the other hand, the results obtained with both methods are in agreement with the previous experimental data and knowledge of laser-induced plasmas (see, e.g., [18–20]).

The line-to-continuum ratio approach is less attractive than the ion-to-neutral ratio approach. The main reason for this is the difficulty of obtaining a sufficient signal-to-noise ratio at the two temporal extremes of the plasma evolution, namely at very early and very late delay times. The former time window precludes the accurate measurement of the line intensity (and therefore an accurate evaluation of the excitation temperature) while the latter precludes the accurate measurement of the continuum. Moreover, Gaunt and Biberman correction factors are needed: in particular, ξ may affect significantly the accuracy of the method. On the other hand, any transition can in principle be used, and therefore the use of a spectrally isolated line and its associated "true" continuum background is facilitated. This is particularly important in the case of a multi-element plasma, since the resulting spectrum will contain a large number of lines, thus necessitating more flexibility in the selection of spectrally isolated lines.

Compared to the line-to-continuum approach, the ion-to-neutral ratio approach is easier to implement at early ($\geqslant \sim 0.5$ μs) and late delay times (~ 5.0 μs), requires calibration of the detection system and the previous evaluation of temperature and electron number density. It should also be stressed that such approach should ideally be applied to a large number of elements characterized by widely different values of the ionization potential. In the present work, the elements investigated are clustered within an interval of 1.05 eV.

Finally, both methods require optically thin plasma conditions and can be advantageously used in space-resolved measurements. When this is not the case, as in the present work, the line-of-sight average information obtained is more difficult to interpret and rationalize.

Acknowledgements

This work was supported by the National Science Foundation through grant CHE-0822469, as part of the Plasma-Analyte Interaction Working Group (PAIWG), a collaborative effort of the University of Florida, Federal Institute of Materials Research and Testing (BAM) in Berlin, and the Institute for Analytical Sciences (ISAS) in Dortmund, jointly funded by the NSF and DFG.

Appendix A

The integrated spectral emissivity (W m^{-3} sr^{-1}), in absence of self-absorption, is given by the following expression:

$$\varepsilon_{line} = \left(\frac{h\nu}{4\pi}\right) A_{u\ell} g_u \left(\frac{n_a}{Z_a}\right) \exp\left(\frac{-E_u}{kT_{exc}}\right). \tag{A1}$$

By using the Saha equilibrium relation, which is given by

$$\frac{n_i n_e}{n_a} = \left(\frac{2Z_i}{Z_a}\right) \frac{(2\pi m k T_{ion})^{3/2}}{h^3} \exp\left(-\frac{E_i - \Delta E_i}{kT_{ion}}\right). \tag{A2}$$

Eq. (A1) becomes:

$$\varepsilon_{line} = C_1 A_{u\ell} \frac{g_u \nu}{Z_i} n_e n_i T_{ion}^{-3/2} \exp\left(\frac{E_i - \Delta E_i}{kT_{ion}} - \frac{E_u}{kT_{exc}}\right), \tag{A3}$$

where

$$C_1 \equiv \left(\frac{h}{8\pi}\right) \frac{h^3}{(2\pi m k)^{3/2}}, \tag{A3a}$$

and is equal to 1.09×10^{-56} [kg m^5 s^{-1} K$^{3/2}$]. Note that the steradian unit has been omitted here. Also, all the symbols have been defined before, except for the atoms (n_a) and ions (n_i) number density, the electron mass (m) and the Planck constant (h).

The expression for the continuum is defined per unit frequency interval, with units of W m^{-3} sr^{-1} Hz^{-1}, and is given by the relation:

$$\varepsilon_{cont}(\nu) = C_2 \frac{n_e n_i}{T_e^{1/2}} \left[\xi\left(1 - \exp\frac{-h\nu}{kT_e}\right) + G \exp\left(\frac{-h\nu}{kT_e}\right)\right], \tag{A4}$$

where

$$C_2 \equiv \frac{16\pi e^6}{3c^3 (6\pi m^3 k)^{1/2}} \times \left(\frac{1}{4\pi\varepsilon_0}\right)^3, \tag{A4a}$$

and is equal to 5.43×10^{-52} [kg m^5 s^{-2} K$^{1/2}$]. Note that the steradian unit is again omitted here, and that e is the electronic charge.

The ratio of Eqs. (A3) and (A5) then results in the expression below:

$$\frac{\varepsilon_{line}}{\varepsilon_{cont}(\nu)} = C_r \frac{A_{u\ell} g_u}{Z_i} \frac{\nu}{T_e} \frac{\exp\left(\frac{-E_u}{kT_{exc}}\right) \exp\left(\frac{E_i - \Delta E_i}{kT_e}\right)}{\left[\xi\left(1 - \exp\frac{-h\nu}{kT_e}\right) + G \exp\left(\frac{-h\nu}{kT_e}\right)\right]}, \tag{A5}$$

where

$$C_r \equiv \left(\frac{C_1}{C_2}\right) \equiv \left(\frac{h^4 3^{3/2} c^3}{256\pi^3 e^6 k}\right), \tag{A5a}$$

is also a known constant, and is equal to 2.005×10^{-5} [s K].

The measured signals are spatially integrated along the line of sight, and weighted by a geometrical collection factor. In addition, the continuum signal is spectrally integrated over the measurement bandwidth of the monochromator. When this is taken into account, the experimental ratio, converted from the frequency domain to the wavelength domain, Eq. (1) is finally obtained:

$$R(\lambda) = C_r \frac{A_{u\ell} g_u}{Z_i} \left(\frac{\lambda}{\Delta\lambda_{meas}}\right) \frac{1}{T_e} \frac{\exp\left(\frac{-E_u}{kT_{exc}}\right) \exp\left(\frac{E_i - \Delta E_i}{kT_e}\right)}{\left[\xi\left(1 - \exp\frac{-hc}{\lambda kT_e}\right) + G \exp\left(\frac{-hc}{\lambda kT_e}\right)\right]}. \tag{A6}$$

Appendix B

The relation between the number of atoms (n_{aj}) and ions (n_{ij}) of species j, the total number of species (n_j) and the degree of ionization (α_j) is given by the well-known relations:

$$n_{i,j} = \alpha_j n_j; \quad n_{a,j} = (1-\alpha_j) n_j, \qquad \frac{n_{i,j}}{n_{a,j}} = \frac{\alpha_j}{(1-\alpha_j)}. \tag{B1}$$

The measured signal intensity for the atomic and ionic (+) transitions are then given by the expressions:

$$(I_{u\ell})_j = (K_{u\ell})_j (1-\alpha_j) n_j \frac{\exp(-E_u/kT)}{(Z_a)_j},$$
$$(I^+_{u\ell})_j = (K^+_{u\ell})_j (\alpha_j) n_j \frac{\exp(-E^+_u/kT)}{(Z_i)_j}, \tag{B2}$$
$$K_{u\ell} \equiv \frac{d}{4\pi} g_u A_{u\ell} h\nu_{u\ell}; \quad K^+_{u\ell} \equiv \frac{d}{4\pi} g^+_u A^+_{u\ell} h\nu^+_{u\ell},$$

where all the terms have been defined before, except for the length of emission d along the line of observation, which is assumed to be homogeneous.

The ion-to-neutral ratio can then be expressed as follows:

$$\frac{(I^+_{u\ell})_j}{(I_{u\ell})_j} = k_1 \cdot k_2 \cdot k_3 \left(\frac{\alpha_j}{1-\alpha_j}\right) = K_{total} \left|\frac{n_{i,j}}{n_{a,j}}\right|, \tag{B3}$$

where

$$k_1 \equiv \left|\frac{g^+_u A^+_{u\ell} h\nu^+_{u\ell}}{g_u A_{u\ell} h\nu_{u\ell}}\right|; \quad k_2 \equiv \left|\frac{Z_{a,j}}{Z^+_j}\right|; \quad k_3 \equiv \exp\left|\frac{E_u - E^+_u}{kT}\right|. \tag{B3a}$$

Using the Saha equilibrium relation:

$$\frac{n_{i,j} n_e}{n_{a,j}} = S_{n,j}(T), \tag{B4}$$

where $S_{n,j}$ is given by Eq. (A2), and combining this equation with Eqs. (B1) and (B3), we obtain:

$$\log \frac{\alpha_j}{1-\alpha_j} = \log \frac{S_{n,j}}{n_e}, \tag{B5}$$

and finally Eq. (2):

$$\log\left[\left(\frac{\alpha_j}{(1-\alpha_j)}\right)\left(\frac{Z_{a,j}}{Z_{i,j}}\right)\right] = \log\frac{S_{n,j}}{n_e} = -\log n_e + \frac{3}{2}\log T - \frac{5040 E_{i,j}}{T} + 15.684. \tag{B6}$$

In the above equation, the last numerical term on the right hand side results from taking the log(base 10) of the ratio $[(2\pi mk)^{3/2}]/(h^3)$, with the constants expressed in cgs units.

References

[1] G. Cristoforetti, A. De Giacomo, M. Dell'Aglio, S. Legnaioli, E. Tognoni, V. Palleschi, N. Omenetto, Spectrochim. Acta B 65 (2010) 86.
[2] R.W.P. McWhirter, in: R.H. Huddlestone, S.L. Leonard (Eds.), Plasma Diagnostic Techniques, Academic Press, New York, 1965, pp. 201–264 (Chapter 5).
[3] M. Capitelli, F. Capitelli, A. Eletskii, Spectrochim. Acta B 55 (2000) 559.
[4] M. Capitelli, A. Casavola, G. Colonna, A. De Giacomo, Spectrochim. Acta B 59 (2004) 271.
[5] D.W. Hahn, N. Omenetto, Appl. Spectrosc. 64 (2010) 335A.
[6] N. Konjević, M. Ivković, S. Jovićević, Spectrochim. Acta B 65 (2010) 593.
[7] C. Aragón, J.A. Aguilera, Spectrochim. Acta B 63 (2008) 893.
[8] G.J. Bastiaans, R.A. Mangold, Spectrochim. Acta B 40 (1985) 885.
[9] A. Sola, M.D. Calzada, A. Gamero, J. Phys. D: Appl. Phys. 28 (1995) 1099.
[10] E. Iordanova, J.M. Palomares, A. Gamero, A. Sola, J.J.A.M. van der Mullen, J. Phys. D: Appl. Phys. 42 (2009) 155208.
[11] H.C. Liu, X.L. Mao, J.H. Yoo, R.E. Russo, Spectrochim. Acta B 54 (1999) 1607.
[12] J.-M. Mermet, Anal. Chim. Acta 250 (1991) 85.
[13] B.L. Caughlin, M.W. Blades, Spectrochim. Acta B 39 (1984) 1583.
[14] C.A. Bye, A. Scheeline, Appl. Spectrosc. 47 (1993) 2022.
[15] I. Holclajtner-Antunović, M. Rašković, S. Jovicević, Spectrochim. Acta B 59 (2004) 419.
[16] A. De Giacomo, M. Dell'Aglio, O. De Pascale, M. Capitelli, Spectrochim. Acta B 62 (2007) 721.
[17] A. De Giacomo, R. Gaudiuso, M. Dell'Aglio, A. Santagata, Spectrochim. Acta B 65 (2010) 385.
[18] M. Milan, J.J. Laserna, Spectrochim. Acta B 56 (2001) 275.
[19] B. Le Drogoff, J. Margot, M. Chaker, M. Sabsabi, O. Barthélemy, T.W. Johnson, S. Laville, F. Vidal, Y. von Kaenel, Spectrochim. Acta B 56 (2001) 987.
[20] O. Barthélemy, J. Margot, S. Laville, F. Vidal, M. Chaker, B. Le Drogoff, T.W. Johnston, M. Sabsabi, Appl. Spectrosc. 59 (2005) 529.
[21] E. Tognoni, M. Hidalgo, A. Canals, G. Cristoforetti, S. Legnaioli, A. Salvetti, V. Palleschi, Spectrochim. Acta B 62 (2007) 435.
[22] P.K. Diwakar, D.W. Hahn, Spectrochim. Acta B 63 (2008) 1038.
[23] C.H. Corliss, J. Res. Natl. Bur. Stand. A: Phys. Chem. 66A (2) (1962) 169.
[24] S. Amoruso, Appl. Phys. A 69 (1999) 323.
[25] P.W.J.M. Boumans, Theory of Spectrochemical Excitation, Plenum Press, New York, 1966.
[26] Heh-Young Moon, K. Herrera, N. Omenetto, B.W. Smith, J.D. Winefordner, Spectrochim. Acta B 64 (2009) 702.
[27] N. Konjević, Phys. Rep. 316 (1999) 339.
[28] W.J. Karzas, R. Latter, Astrophys. J. (1961) 167.
[29] H. Van Regenmorter, Astrophys. J. 136 (1962) 906.
[30] R.C. Elton, in: H.R. Griem, R.H. Lovberg (Eds.), Methods of Experimental Physics, Part A, vol. 9, Academic Press, New York, London, 1970.
[31] S. Manola, S. Devic, A. Lesage, J. Quant. Spectrosc. Rad. Transfer 46 (6) (1991) 577.
[32] A.T.M. Wilbers, G.M.W. Kroesen, C.J. Timmermans, D.C. Schram, J. Quant. Spectrosc. Rad. Transfer 45 (1) (1991) 1.
[33] A.A. Pupyshev, E.V. Semenova, Spectrochim. Acta B 56 (2001) 2397.
[34] C.Th.J. Alkemade, Tj. Hollander, W. Snelleman, P.J.Th. Zeegers, Metal Vapours in Flames, Pergamon Press, Oxford, 1982. p. 55.